Effects of the positron spatial distribution on momentum densities in random muffin-tin alloys

A. Bansil
Department of Physics, Northeastern University, Boston, Massachusetts 02115

P. E. Mijnarends
Netherlands Energy Research Foundation ECN, 1755 ZG Petten, The Netherlands

(Received 3 August 1983)

We consider the problem of incorporating positron spatial distribution effects on the two-photon momentum density $\langle \rho_{2\gamma}(\vec{p}) \rangle$ in a disordered alloy. $\langle \rho_{2\gamma}(\vec{p}) \rangle$ formally involves the average $\langle GG_+ \rangle$ of the product of electron and positron Green's functions. Our approach utilizes the framework of the average-t-matrix and coherent-potential approximations to treat disorder in the alloy and neglects the vertex corrections which arise in evaluating $\langle GG_+ \rangle$. The influence of disorder on the positron state is delineated in terms of the properties of $\langle G_+ \rangle$. Illustrative results for Cu, $Cu_{75}Ni_{25}$, $Cu_{50}Ni_{50}$, and Ni are presented and discussed.

I. INTRODUCTION

The recent development of the technique of two-dimensional angular correlation of annihilation radiation[1-3] (2D-ACAR) has provided a powerful tool for the investigation of the electronic structure of disordered alloys. Several detailed studies of alloy Fermi surfaces using 2D-ACAR have already been reported.[4-6] On the theoretical side, the average-t-matrix (ATA) and coherent-potential (CPA) approximations[7-12] have been used to calculate the configurationally averaged momentum density $\langle \rho(\vec{p}) \rangle$ in a disordered muffin-tin alloy. Most calculations reported so far, however, neglect the influence of the positron or, equivalently, assume the positron spatial distribution to be uniform. Hence, the resulting momentum densities are related to Compton scattering experiments rather than to measured ACAR's.[13] Therefore, the need to incorporate the effects of the positron in momentum-density calculations in alloys is clear. Hong and Carbotte[14] have previously considered this question within the framework of a single band model Hamiltonian. The present paper is an attempt to address the problem in a realistic manner by employing the appropriate muffin-tin Hamiltonians to treat the electron as well as the positron states in the system. Illustrative results for Cu-Ni alloys are presented and discussed.

The outline of this paper is as follows. Section II discusses the properties of a single thermalized positron placed in a random alloy of (repulsive) muffin-tin potentials.[15] This problem can be dealt with by the familiar ATA and CPA techniques and provides a considerable insight into the characteristic effects of disorder on the positron. Computations of the positron spectral density $\langle \rho_+(\vec{p},E) \rangle$ and the associated temperature-dependent momentum density $\langle N_+(\vec{p},T) \rangle$ at 4 and 300 K in $Cu_{50}Ni_{50}$ are presented. We comment on the qualitative differences which exist in the way positrons and electrons sample the disorder in an alloy.

Section III discusses the electron-positron momentum density $\langle \rho_{2\gamma}(\vec{p}) \rangle$, relevant for analyzing the measured ACAR's. $\langle \rho_{2\gamma}(\vec{p}) \rangle$ formally involves the average $\langle GG_+ \rangle$ of the product of electron and positron Green's functions and is thus intrinsically a more complicated quantity than the one-particle properties (i.e., those involving only $\langle G \rangle$). The simplest approach is to replace $\langle GG_+ \rangle$ by $\langle G \rangle \langle G_+ \rangle$. We use this approximation to obtain a practical scheme for evaluating $\langle \rho_{2\gamma}(\vec{p}) \rangle$ in an alloy. Results for $\langle \rho_{2\gamma}(\vec{p}) \rangle$ and the electron momentum density $\langle \rho(\vec{p}) \rangle$ in Cu, $Cu_{75}Ni_{25}$, $Cu_{50}Ni_{50}$, and Ni are presented and discussed. The vertex corrections neglected by using $\langle GG_+ \rangle \approx \langle G \rangle \langle G_+ \rangle$ will be important in situations of a strong positron affinity for one of the constituents.[16,17] We comment on this question and on an alternative scheme for decoupling the average $\langle GG_+ \rangle$. It should be noted that the present treatment implicitly assumes electrons and positrons to be independent particles and does not include effects of electron-positron correlations.

II. THE POSITRON STATE

The nature of the positron state can be explored by considering the properties of a single thermalized positron placed in the disordered alloy A_xB_{1-x}.[15] The relevant one-particle Hamiltonian is

$$H_+ = p^2/2m + \sum_n V_n^{(+)}(r) \, . \tag{1}$$

In analogy with the electronic problem, the potentials $V_A^{(+)}$ and $V_B^{(+)}$ are assumed to possess a nonoverlapping muffin-tin form and to occupy the lattice sites randomly. But, in contrast to the electronic case, the $V_n^{(+)}$ are repulsive and do not contain an exchange contribution. The one-particle properties can be discussed within the framework of the ATA and CPA. For example, the average density of states is given in terms of the configurationally

averaged positron Green's function $\langle G_+ \rangle$ by

$$\langle \rho_+(E) \rangle = -\pi^{-1} \mathrm{Im}\, \mathrm{Tr} \langle G_+ \rangle \ . \tag{2}$$

The spectral momentum density is

$$\langle \rho_+(\vec{p},E) \rangle = -\pi^{-1} \mathrm{Im} \langle G_+(\vec{p},\vec{p};E) \rangle \ , \tag{3}$$

and is shown in Fig. 1 for $Cu_{50}Ni_{50}$.[18] The energy positions of the peaks together with the associated values of $\vec{p}$ define a positron band. In a perfect crystal these peaks would be δ functions; the finite width of the spectral peaks in Fig. 1 indicates the disorder smearing of the positron in the alloy. The CPA spectral peaks become sharper for decreasing p and culminate in an edge at $p=0$. The CPA density of states $\langle \rho_+(E) \rangle$ in fact vanishes for $E < E_0 = 0.501\,43$ Ry; a proof of the existence of such an edge is provided in Appendix A. The ATA, on the other hand, does not provide a sharp band edge and the ATA peaks near $p=0$ are substantially broader than those of the CPA.

For a thermalized positron at temperature T, the physically relevant momentum density $\langle N_+(\vec{p},T) \rangle$ is obtained with the aid of the Boltzmann factor $f_+(E)$:

$$\langle N_+(\vec{p},T) \rangle = \int_{-\infty}^{\infty} dE\, f_+(E) \langle \rho_+(\vec{p},E) \rangle \ . \tag{4}$$

Figure 2 shows $\langle N_+(\vec{p},T) \rangle$ at 4 and 300 K in $Cu_{50}Ni_{50}$. It has been computed assuming an effective mass of unity. Since it involves only momenta close to $p=0$, it is practically entirely determined by the s-phase shifts of the constituents. Moreover, it is virtually isotropic in cubic materials. As will become apparent in the next section, $\langle N_+(\vec{p},T) \rangle$ is convoluted with the electron momentum density and thus acts as a temperature- and disorder-dependent smearing function. The closeness of the (solid) CPA curve in Fig. 2 to the positron momentum distribution due to thermal motion alone (dashed curve; this effect is present even in a perfect crystal[19]) indicates that the disorder smearing in CuNi alloys is rather small. This is not surprising since Cu and Ni scatter the positron in much the same way (see also Ref. 12).

Owing to the presence of the Boltzmann factor $f_+(E)$ in the integrand of Eq. (4), the function $\langle N_+(\vec{p},T) \rangle$ depends sensitively on the detailed shape of the positron spectral density $\langle \rho_+(\vec{p},E) \rangle$. In particular, if the ATA were used to calculate $\langle N_+(\vec{p},T) \rangle$, the Boltzmann factor would impart an unphysically large weight to the long low-energy Lorentzian tail of $\langle \rho_+(\vec{p},E) \rangle$ (see the lower part of Fig. 1). The CPA, on the other hand, yields a band edge and hence a well-defined momentum density at all temperatures. Although the ATA cannot be used to calculate the shape of $\langle N_+(\vec{p},T) \rangle$, it is still a reasonable

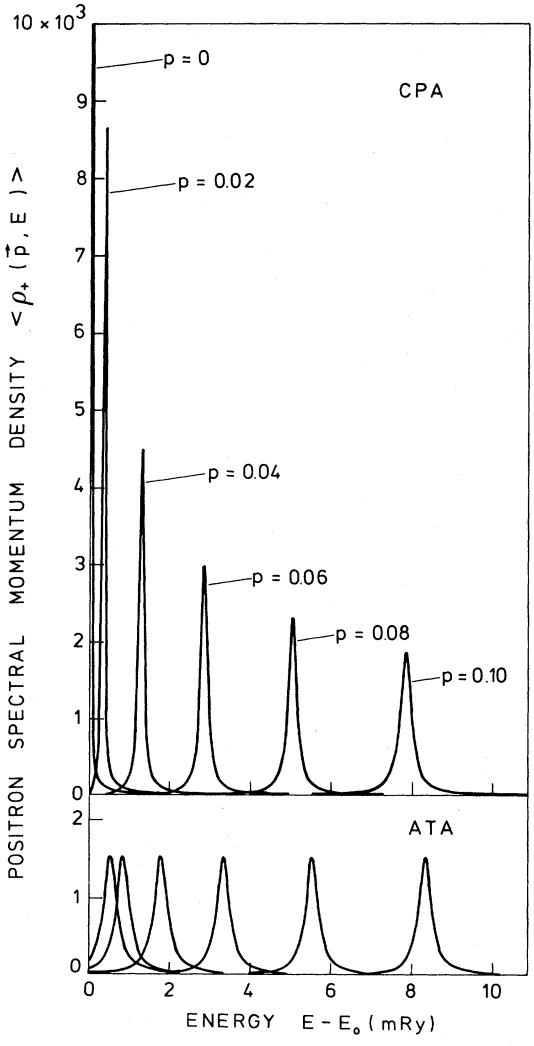

FIG. 1. CPA (upper part) and ATA (lower part) positron spectral momentum densities $\langle \rho_+(\vec{p},E) \rangle$ in $Cu_{50}Ni_{50}$ for momenta $\vec{p}$ along the $\langle 100 \rangle$ direction. The curves in the lower part correspond to the same p values as the curves in the upper part. Energies on the horizontal scale are given with respect to the CPA band edge at $E_0 = 0.501\,43$ Ry.

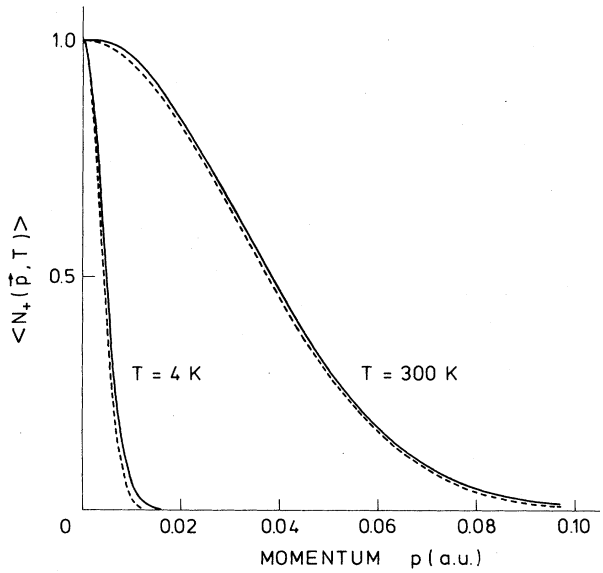

FIG. 2. CPA positron momentum density $\langle N_+(\vec{p},T) \rangle$ [see Eq. (4)] for $\vec{p}$ along the $\langle 100 \rangle$ direction in $Cu_{50}Ni_{50}$ at 4 and 300 K (solid). The dashed curves give the effect of thermal motion alone.

scheme for obtaining the Fourier components of the (average) spatial distribution of the positron in the alloy. We shall return to this point in the following section.

It is important to recognize that the positron sees the disorder in an alloy in a manner which differs qualitatively from the electrons. The positron is repelled by the ions and tends to sample the outer parts of the Wigner-Seitz cell, whereas the electrons are attracted toward the ionic cores. Also, the positron occupies states near the bottom of the positron conduction band, while the electron conduction band is filled up to the Fermi energy. In the preceding example of CuNi, the effective disorder experienced by electronic states of d symmetry is large (i.e., separate Cu and Ni d subbands appear in the alloy), but states of s and p symmetry are hardly affected by alloying. The behavior of the positron being related to that of the s-type electronic levels at the bottom of the valence bands, the effects of disorder on the positron were seen above to be quite small in CuNi.[20] Larger effects may be expected in alloys in which the s-phase shifts of the constituents are greatly different [e.g., CuGe (Ref. 21) and CuAl (Ref. 22)].

III. TWO-PHOTON MOMENTUM DISTRIBUTION

The configurationally averaged electron-positron momentum density for two-photon annihilation, $\langle\rho_{2\gamma}(\vec{p})\rangle$, can be cast in terms of the electron and positron Green's functions as[13,14]

$$\langle\rho_{2\gamma}(\vec{p})\rangle=\frac{1}{\pi^2}\int d\vec{r}\int d\vec{r}\,'\exp[-i\vec{p}\cdot(\vec{r}-\vec{r}\,')]\int dE\,f(E)\int dE_+ f_+(E_+)\langle \mathrm{Im}G(\vec{r},\vec{r}\,';E)\mathrm{Im}G_+(\vec{r},\vec{r}\,';E_+)\rangle\ , \tag{5}$$

where the subscript $+$ refers to positron quantities. The Fermi-Dirac function $f(E)$, which gives the occupation probability for the electronic levels, degenerates to the Maxwell-Boltzmann distribution $f_+(E_+)$ for the low-density positron state. To evaluate the complicated integrand of Eq. (5), the simplest approximation is to replace the average of the product of G and G_+ by the product of their averages:

$$\langle \mathrm{Im}G\,\mathrm{Im}G_+\rangle\approx\mathrm{Im}\langle G\rangle\mathrm{Im}\langle G_+\rangle\ . \tag{6}$$

The terms left out in writing decoupling (6), often referred to as vertex corrections, physically describe the fact that the positron and the electron respond to the *same* configuration of A and B atoms (rather than to an average one) before they annihilate.[23] When the positron samples both types of atoms in a comparable manner (as in CuNi) one can expect the decoupling (6) to be a reasonable approximation. On the other hand, the vertex corrections will be particularly important in situations where the positron shows a marked affinity for one of the constituents. The case of positron trapping in crystals with defects (e.g., vacancies[24]) is an extreme example. In the following we shall utilize approximation (6) and later on return briefly to the question of the vertex corrections.

Using the convolution theorem, Fourier transformation of Eq. (5), with Eq. (6), yields

$$\langle\rho_{2\gamma}(\vec{p})\rangle=\frac{1}{\pi^2}\int dE\,f(E)\int dE_+ f_+(E_+)\int\frac{d\vec{s}}{(2\pi)^3}\int\frac{d\vec{t}}{(2\pi)^3}\langle \mathrm{Im}G(\vec{p}-\vec{s},\vec{p}-\vec{t}\,;E)\rangle\langle \mathrm{Im}G_+(\vec{s},\vec{t}\,;E_+)\rangle\ . \tag{7}$$

The electron and positron Green's functions in Eq. (7) are given by a straightforward generalization involving the nondiagonal elements of the previously derived momentum-density expressions for Compton scattering:[7–9]

$$\langle \mathrm{Im}G(\vec{p},\vec{q};E)\rangle=\mathrm{Im}\left\{\frac{\delta_{\vec{p}-\vec{q}}}{E-p^2}+\sum_{\vec{G}}\frac{(4\pi)^2N\delta_{\vec{p}-\vec{q},\vec{G}}}{(E-p^2)(E-q^2)}\sum_{LL'}Y_L(\hat{p})\left[\left[t_l(p,q)-\frac{t_l(p,\kappa)t_l(\kappa,q)}{t_l(\kappa,\kappa)}\right]\delta_{LL'}\right.\right.$$
$$\left.\left.+\frac{t_l(p,\kappa)}{t_l(\kappa,\kappa)}[t(\kappa,\kappa)^{-1}-B(\vec{p},E)]^{-1}_{LL'}\frac{t_{l'}(\kappa,q)}{t_{l'}(\kappa,\kappa)}\right]Y_{L'}(\hat{q})\right\}. \tag{8}$$

Here $\kappa\equiv\sqrt{E}$ and $L\equiv(l,m)$ is a composite angular momentum index. N is the total number of lattice sites per unit of volume. Y_L denotes a real spherical harmonic, $\vec{G}$ a reciprocal lattice vector, and $B(\vec{p},E)$ the matrix of Korringa-Kohn-Rostoker (KKR) structure functions. Since the underlying crystal lattice is periodic, $B(\vec{p},E)$ is a periodic function in reciprocal space and, as $\vec{p}$ and $\vec{q}$ in Eq. (8) are only allowed to differ by a reciprocal lattice vector, $B(\vec{p},E)=B(\vec{q},E)=B(\vec{k},E)$, where $\vec{k}$ is the reduced wave vector corresponding to $\vec{p}$ and $\vec{q}$. Applying this to the positron part of Eq. (7) one obtains[13]

$$\langle\rho_{2\gamma}(\vec{p})\rangle=\frac{1}{\pi^2}\sum_{\vec{k}_+}\int dE\,f(E)\int dE_+ f_+(E_+)\sum_{nn'}\langle \mathrm{Im}G(\vec{p}-\vec{k}_+-\vec{K}_n,\vec{p}-\vec{k}_+-\vec{K}_{n'};E)\rangle$$
$$\times\langle \mathrm{Im}G_+(\vec{k}_++\vec{K}_n,\vec{k}_++\vec{K}_{n'};E_+)\rangle\ . \tag{9}$$

This formula, together with Eq. (8), allows the calculation of $\langle \rho_{2\gamma}(\vec{p}) \rangle$.

The structure of Eq. (9) is that of a two-dimensional convolution of the electron and positron momentum densities, i.e., after the energy integrations, Eq. (9) expresses $\langle \rho_{2\gamma}(\vec{p}) \rangle$ as a sum over $\vec{k}_+$ of a product of electron and positron matrices in $(\vec{K}_n, \vec{K}_{n'})$ space.[25] The positron momentum density consists of a set of peaks of the form of Eq. (4), centered at the reciprocal lattice points. Their relative weights give the Fourier components of the average spatial distribution of the positron in the alloy and describe the deviation of this distribution from a constant. In the limit of a perfect crystal at $T=0$ K, the peaks become δ functions and only the positron state with $\vec{k}_+=0$ and electron levels with reduced $\vec{k}=\vec{p}-\vec{K}$ (where $\vec{K}$ is the reciprocal lattice vector which reduces $\vec{p}-\vec{k}_+$ to the first Brillouin zone) contribute to $\langle \rho_{2\gamma}(\vec{p}) \rangle$. In the alloy, on the other hand, even at $T=0$ K, Eq. (9) implies that a *range* of positron momenta around $\vec{k}_+=0$ together with the associated electronic momenta $\vec{k}=\vec{p}-\vec{k}_+-\vec{K}$ will be involved. This is a consequence of the disorder-induced smearing of levels and cannot be avoided.

Another remark concerns the first term in Eq. (8). This apparent free-electron pole does not lead to singular behavior near $E=p^2$ since it cancels a similar contribution[7,9] from the last term in Eq. (8) as $E \to p^2$.

Figure 3 displays representative two-photon momentum densities at $T=0$ K in Cu, $Cu_{75}Ni_{25}$, $Cu_{50}Ni_{50}$, and Ni

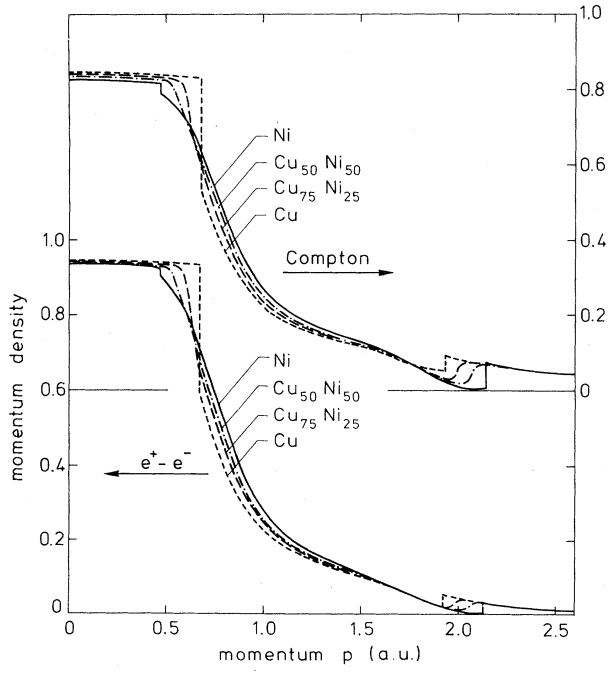

FIG. 3. Electron momentum densities $\langle \rho(\vec{p}) \rangle$ for Compton scattering and electron-positron momentum densities $\langle \rho_{2\gamma}(\vec{p}) \rangle$ for two-photon annihilations at $T=0$ K in Cu, $Cu_{75}Ni_{25}$, $Cu_{50}Ni_{50}$, and Ni, along the $\langle 110 \rangle$ direction. See text for computational details.

along the $\langle 110 \rangle$ direction, together with the corresponding results for Compton scattering. The two sets of curves are quite similar, apart from the expected more rapid decrease of the e^+-e^- density at high momenta caused by the nuclear repulsion of the positron. In going from Ni to Cu, the break in the first zone (at approximately 0.5 a.u.) moves farther to the right and becomes more pronounced, reflecting an increase in the $\langle 110 \rangle$ Fermi surface radius and in the *s-p* character of the associated states. The rounding of structures in the alloy curves is a result of the *electron*-disorder scattering; as noted earlier, the effect of the positrons in this regard is negligible. For the 50-50 alloy, we estimate the disorder-induced smearing (width) $|2\Delta\vec{k}|$ of the $\langle 110 \rangle$ radius to be approximately 0.04 a.u. This is about four times larger than the total width of the positron momentum density at 4 K (see Fig. 2), and just at the current limit of detection in a high-resolution 2D-ACAR experiment. Much of the preceding discussion is also applicable (with obvious modifications) to Fig. 4, which shows the momentum density along the off-the-zone-center direction joining the (111) and (113) reciprocal lattice points. We have previously presented the Compton density along this direction in order to explore the nature of the dip at about 1.8 a.u.; this dip is related to the appearance of *d*-hole pockets around the symmetry point *X* in the Ni-rich alloys.[7,9] Figure 4 shows that this feature continues to be seen clearly in the alloy, even though it becomes less pronounced when positron spatial distribution effects are included.

Concerning computational details, we note that the fact that the disorder smearing of the positron in CuNi alloys is quite small permitted simplifications in the evaluation of $\langle \rho_{2\gamma}(\vec{p}) \rangle$. First of all, it was found that the peaks in the positron Green's function, centered at the reciprocal lattice points, to a high approximation all have the same shape. They only differ by scaling factors, which are given by the Fourier coefficients. The latter vary by less than half a percent between 4 K and room temperature. Therefore, in the first instance the broadening of the peaks was neglected altogether [i.e., $\langle G_+(\vec{k}_+ + \vec{K}_n, \vec{k}_+ + \vec{K}_{n'}) \rangle$ was replaced by $\langle G_+(\vec{K}_n, \vec{K}_{n'}) \rangle$]. The positron temperature and disorder broadening can then be introduced at the end of the calculation by convoluting $\langle \rho_{2\gamma}(\vec{p}) \rangle_{T=0}$ with the smearing function $\langle N_+(\vec{p},T) \rangle$ of Eq. (4).

Secondly, it should be emphasized that the Green's functions in the integrand of Eq. (9) possess strongly peaked structures [due to the inverse matrix $(t^{-1}-B)^{-1}$ in Eq. (8)] and must be evaluated at many energies. This makes the summation over n and n' a very cumbersome one. However, the calculations can be speeded up considerably by realizing that the $\vec{K}_n, \vec{K}_{n'}$ dependence in Eq. (9), keeping in mind the form of Eq. (8), is separable to a good approximation. This allows the double summation over n,n' to be replaced by two identical single summations. Further details with respect to this point can be found in Appendix B. Finally, important gains in computational speed were obtained by the extensive use of interpolation in the evaluation of the structure functions and the t matrices.[7,9,26,27]

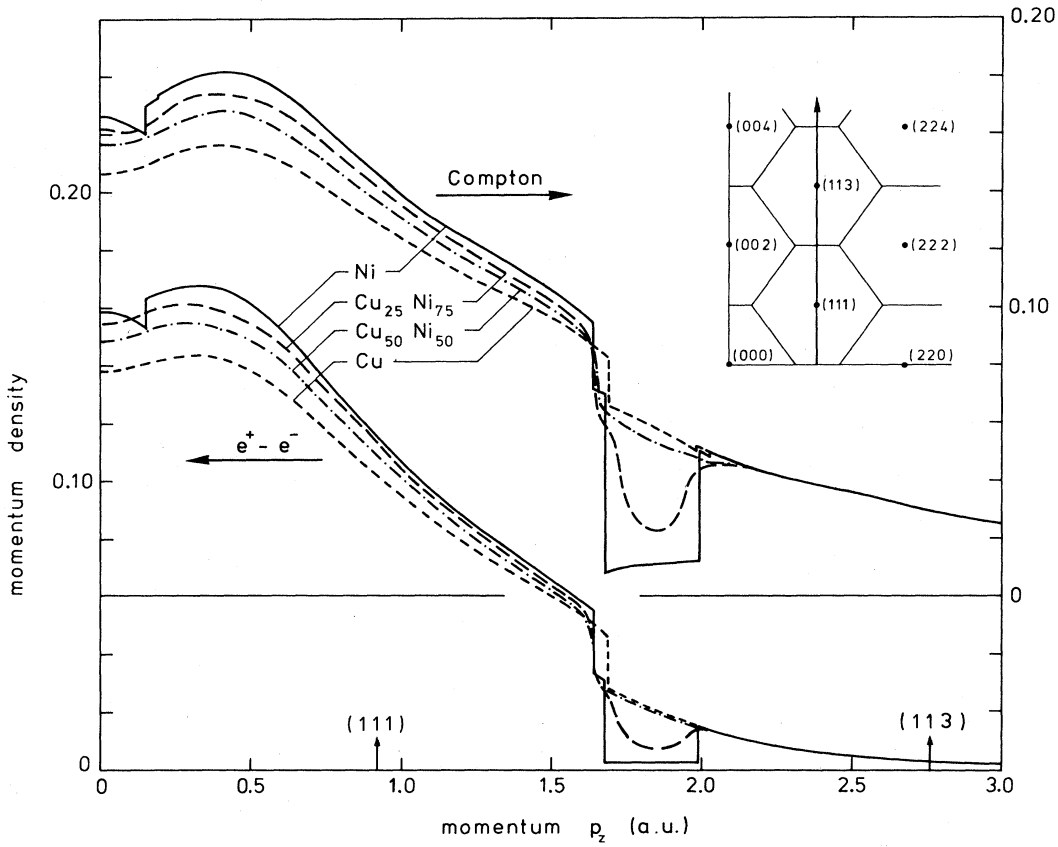

FIG. 4. Same as the caption to Fig. 3, except that this figure gives momentum densities along the off-the-zone-center direction (see inset) joining the (111) and (113) reciprocal lattice points.

A point deserving comment is the use of the CPA versus the ATA. Equation (8) is applicable to either the CPA or the ATA depending on the choice of the effective atom scattering matrices $t_l(p,q)$.[7,9] The CPA treats disorder self-consistently and is therefore obviously to be preferred over the (computationally simpler) ATA. However, it has been shown that, although CPA and ATA yield markedly different results for the spectral quantity $\langle\rho(\vec{p},E)\rangle$, they produce practically indistinguishable values of the electron momentum density:[7-9]

$$\langle\rho(\vec{p},T)\rangle \propto \int_{-\infty}^{\infty} dE\, f(E)\langle\rho(\vec{p},E)\rangle \ . \tag{10}$$

The reason is that the energy integration in (10) is weighted by the Fermi-Dirac function $f(E)$ which, excepting an interval of width kT around the Fermi energy, is a constant. Consequently, $\langle\rho(\vec{p},T)\rangle$ is determined mainly by the spectral weights of the peaks in $\langle\rho(\vec{p},E)\rangle$ and is not sensitive to their shapes. The electron part of Eq. (9) can thus be computed generally within the simpler ATA theory to a good approximation. The situation with the positron part of $\langle\rho_{2\gamma}(\vec{p})\rangle$ on the other hand is more delicate. It was pointed out in connection with Fig. 2 above that the distribution $\langle N_+(\vec{p},T)\rangle$ cannot be obtained reliably using the ATA. But, we have seen that the positron also affects $\langle\rho_{2\gamma}(\vec{p})\rangle$ via its lattice Fourier coefficients, which depend on the spectral weights associated with the peaks in $\langle\rho_+(\vec{p},E)\rangle$. As in the electronic case, these weights are in general given reasonably by the ATA. These procedures were followed in obtaining the momentum-density results in Figs. 3 and 4. They correspond thus to the use of the CPA in the positron part and the ATA in the electron part of Eq. (9). However, as indicated above the present results are expected to be close to what would be obtained if the CPA were used for the electron part also.

We return finally to the question of vertex corrections, neglected in writing the approximate form (6). Similar corrections arise more generally in the treatment of a variety of physical properties of alloys, most notably the transport coefficients. While systematic methods should be brought to bear on this problem,[17] it may also be useful to consider the following decoupling:

$$\langle \mathrm{Im}G\ \mathrm{Im}G_+\rangle \rightarrow x\ \mathrm{Im}G^A\mathrm{Im}G_+^A + (1-x)\mathrm{Im}G^B\mathrm{Im}G_+^B \ , \tag{11}$$

where $G^{A(B)}$ (or $G_+^{A(B)}$) denotes the electron (or positron) Green's function for a single $A(B)$ impurity embedded in the effective medium. Like decoupling (6), the form on the right-hand side of (11) can in principle be evaluated by

the existing ATA and CPA techniques. Also, the form (11) can be viewed as a first step in a self-consistent cluster-type generalization of the KKR-CPA theory. In any event, a comparison of the $\langle \rho_{2\gamma}(\vec{p}) \rangle$ values based on Eqs. (11) and (6) would allow insight into the nature and importance of vertex corrections in realistic systems.

ACKNOWLEDGMENTS

We are grateful to Dr. L. Schwartz, Dr. R. Prasad, and Dr. R. S. Rao for important conversations. This work was supported in part by the National Science Foundation.

APPENDIX A: EXISTENCE OF A LOW-ENERGY BAND EDGE IN THE MUFFIN-TIN CPA

The CPA density of states can be written as[27]

$$\langle \rho(E) \rangle = \rho_0(E) - \frac{1}{\pi N} \mathrm{Im\,Tr} \sum_{\vec{k}} \left[\frac{C_B - C}{C_B - C_A} \frac{dC_A}{dE} + \frac{C_A - C}{C_A - C_B} \frac{dC_B}{dE} + \frac{dA_{\vec{k}}}{dE} \right] \left[\frac{1}{A_{\vec{k}} + C} \right] . \tag{A1}$$

Here, much of the notation is obvious; the trace refers to the angular momentum space. C_A, C_B, and C, respectively, denote the matrices of $\sqrt{E}$ times the cotangents of the A, B, and CPA phase shifts. C_A and C_B are real, while C is in general complex. $A_{\vec{k}}$ is the matrix of real KKR structure constants: $A_{\vec{k}}(E) \equiv B(\vec{k},E) - i\sqrt{E}$. The quantities C are given by the CPA equation[27]

$$C = xC_A + yC_B + (C - C_A) f(C) (C - C_B) , \tag{A2}$$

where $y = 1 - x$ and

$$f(C) \equiv N^{-1} \sum_{\vec{k}} (C + A_{\vec{k}})^{-1} . \tag{A3}$$

Since we are interested in the low-energy band edge, we restrict ourselves to the case of only the s-phase shifts; various matrices in the preceding equations then become scalar functions. Note that, at a given E, if $C'' \equiv \mathrm{Im}C = 0$ and $(A_{\vec{k}} + C) \neq 0$ for all $\vec{k}$, then Eq. (A1) implies $\langle \rho(E) \rangle = 0$. [Contributions from the free-electron singularities of $A_{\vec{k}}(E)$ cancel against $\rho_0(E)$ exactly and are therefore not considered.] $C'' = 0$ obviously satisfies Eq. (A2) provided $\mathrm{Im}f(C) = 0$. Under these conditions, $C' = \mathrm{Re}C$ is given by the equation

$$F(C') \equiv C' - xC_A - yC_B - (C' - C_A) f(C') (C' - C_B) = 0 . \tag{A4}$$

But $F(C')$ changes sign between $C' = C_A$ and $C' = C_B$ and thus possesses a zero in this range. Therefore, assuming reasonably behaved functions, if $(C_A + A_{\vec{k}})$ and $(C_B + A_{\vec{k}})$ do not vanish at the energy in question, $(C' + A_{\vec{k}})$ will also not vanish and $\mathrm{Im}C = 0$, $\mathrm{Im}f(C) = 0$ is a solution of the CPA equation. These conditions will be satisfied at energies lying below the bottoms of both pure A and B bands, and $\langle \rho(E) \rangle = 0$ is the physical solution in this regime. This result is similar to the localization theorem in the case of a single-tight-binding band alloy. The ATA, on the other hand, yields

$$\mathrm{Im}C^{\mathrm{ATA}} = - \left[\frac{xy(C_A - C_B)^2}{1 + (xC_B + yC_A)^2} \right] < 0 \quad \text{for } E > E_{\mathrm{MT}} , \tag{A5}$$

where E_{MT} is the muffin-tin zero. This result is readily obtainable from $t^{\mathrm{ATA}} = xt_A + yt_B$, with $t_\alpha^{-1} = \kappa(i - C_\alpha)$, and $\alpha = A$, B, or ATA. Equation (A5) implies a nonvanishing density of states at all energies above the muffin-tin zero.

APPENDIX B: SEPARABILITY OF THE $\vec{K}_n, \vec{K}_{n'}$ DEPENDENCE

The approximate separability of the $\vec{K}_n, \vec{K}_{n'}$, dependence in Eq. (9) is seen by considering in Eq. (8) the terms in parentheses multiplying $\delta_{LL'}$ and the terms containing $(t^{-1} - B)^{-1}$ separately, and calling them U^- and V^- in the electron case, and U^+ and V^+ in the positron case, respectively. In V^- and V^+, $\vec{K}_n$ and $\vec{K}_{n'}$ only enter via the multiplicative side factors of the form

$$Y_L(\hat{p}) [t_l(p,\kappa)/t_l(\kappa,\kappa)] (E - p^2)^{-1} .$$

In V^+, these side factors vary only little over the width of the Boltzmann distribution $f_+(E_+)$ of the positron and they may therefore, to a good approximation, be taken out of the integration with respect to E_+ in Eq. (9). The terms U^- and U^+, on the other hand, are not separable owing to the occurrence of $t_l(p,q)$. However, for a positron in $Cu_{1-x}Ni_x$, U^+ is much smaller than V^+ and hence the error made in approximating

$$\int f_+(E_+) \langle \mathrm{Im}G_+ \rangle dE_+$$

by an expression of the form

$$\sum_{\Lambda\Lambda'} g_\Lambda(\vec{K}_n) M_{\Lambda\Lambda'} g_{\Lambda'}(\vec{K}_{n'})$$

is unimportant. Here, $M_{\Lambda\Lambda'}$ contains the integration with respect to the positron energy E_+, and Λ and Λ' are the positron equivalents of the electron angular momentum indices L and L'. The result of the separation of the $\vec{K}_n, \vec{K}_{n'}$ dependence in

$$\int f_+(E_+) \langle \mathrm{Im}G_+ \rangle dE_+$$

and in V^- is that at every energy E the double summation over n,n' can now be written as the product of two identical single summations, each of these summations resulting in a matrix in (L,Λ) space. If necessary, the electron terms of the type U^- can be treated separately.

Generally, these terms are small and structureless, and it suffices to perform computations invoking the double summation over n,n' at a relatively small number of $(E,\vec{p})$ points. In CuNi their contribution to $\langle\rho_{2\gamma}(\vec{p})\rangle$ is nowhere higher than a few times 10^{-5} and hence they were neglected altogether. Owing to the fairly rapid convergence of the positron Fourier expansion, the summations over n,n' were limited to the first 27 reciprocal lattice vectors. This gave an accuracy better than 0.1% up to $p=2$ a.u. Further gains in computational speed were obtained by restricting the positron angular momentum summation to $\Lambda=0$ (only s states at Γ_1).

[1]S. Berko, M. Haghgooie, and J. J. Mader, Phys. Lett. 63A, 335 (1977).

[2]A. A. Manuel, S. Samoilov, Ø. Fischer, and M. Peter, Helv. Phys. Acta 52, 255 (1979).

[3]R. N. West, J. Mayers, and P. A. Walters, J. Phys. E 14, 478 (1981).

[4]S. Berko and J. Mader, Appl. Phys. 5, 287 (1975).

[5]S. Berko and J. Mader, Phys. Condens. Matter 19, 405 (1975); S. Berko, M. Haghgooie, and J. J. Mader, in *Physics of Transition Metals, 1977,* edited by M. J. G. Lee, J. M. Perz, and E. Fawcett, Conference Series No. 39 (Institute of Physics, Bristol, 1978), p. 94; M. Haghgooie, S. Berko, and U. Mizutani, in *Positron Annihilation,* edited by R. R. Hasiguti and K. Fujiwara (Japan Institute of Metals, Sendai, 1979), p. 291.

[6]A. A. Manuel, L. Oberli, T. Jarlborg, R. Sachot, P. Descouts, and M. Peter, in *Positron Annihilation,* edited by P. G. Coleman, S. C. Sharma, and L. M. Diana (North-Holland, Amsterdam, 1982), p. 281.

[7]P. E. Mijnarends and A. Bansil, Phys. Rev. B 13, 2381 (1976); 19, 2912 (1979).

[8]A. Bansil, R. S. Rao, P. E. Mijnarends, and L. Schwartz, in *Physics of Transition Metals, 1980,* edited by P. Rhodes, Conference Series No. 55 (Institute of Physics, Bristol, 1981), p. 49.

[9]A. Bansil, R. S. Rao, P. E. Mijnarends, and L. Schwartz, Phys. Rev. B 23, 3608 (1981).

[10]B. L. Gyorffy and G. M. Stocks, J. Phys. F 10, L321 (1980).

[11]B. E. A. Gordon, W. E. Temmerman, and B. L. Gyorffy, J. Phys. F 11, 821 (1981).

[12]Z. Szotek, B. L. Gyorffy, G. M. Stocks, and W. M. Temmerman, in *Positron Annihilation* (Ref. 6), p. 251.

[13]P. E. Mijnarends, in *Positron Solid-State Physics,* edited by W. Brandt and A. Dupasquier (North-Holland, Amsterdam, 1983), p. 146.

[14]K. M. Hong and J. P. Carbotte, Can. J. Phys. 55, 1335 (1977).

[15]A. Bansil, in *Positron Annihilation* (Ref. 6), p. 291.

[16]B. L. Gyorffy, in *Physics of Transition Metals, 1980* (Ref. 8), p. 89.

[17]L. Schwartz, Phys. Rev. B 24, 1091 (1981).

[18]We have employed inverted Cu and Ni electron muffin-tin potentials for the positron. The exchange contributions, which are thus not excluded, are comparable in Cu and Ni and are estimated to have a small effect on the present results in CuNi.

[19]A. T. Stewart and J. B. Shand, Phys. Rev. Lett. 16, 261 (1966).

[20]In view of this discussion, the use of essentially the same disorder parameter (except for sign) for the positron as well as the electrons in the single-band model calculations of Hong and Carbotte (Ref. 14) is not realistic in transition and noble metal alloys.

[21]R. Prasad and A. Bansil, Phys. Rev. Lett. 48, 113 (1982).

[22]H. Asonen, M. Lindroos, M. Pessa, R. Prasad, R. S. Rao, and A. Bansil, Phys. Rev. B 25, 7075 (1982).

[23]Approximation (6) is concerned with the treatment of disorder and is distinct from the usual assumption of independent particles. Equations (5) and (6) implicitly neglect correlation effects between the positron and electrons.

[24]See, for example, R. M. Nieminen, in *Positron Solid-State Physics,* edited by W. Brandt and A. Dupasquier (North-Holland, Amsterdam, 1983), p. 359.

[25]A similar KKR formula for $\rho_{2\gamma}(\vec{p})$ in a perfect crystal is given in Ref. 13.

[26]G. M. Stocks, W. M. Temmerman, and B. L. Gyorffy, in *Electrons in Disordered Metals and at Metallic Surfaces,* edited by P. Phariseau, B. L. Gyorffy, and L. Scheire (Plenum, New York, 1979), p. 193.

[27]A. Bansil, Phys. Rev. B 20, 4025 (1979); 20, 4035 (1979); 23, 3107(E) (1981).